applied sciences

MDPI

Article

Clutter Suppression Algorithm with Joint Intrinsic Clutter Motion Errors Calibration and Off-Grid Effects Mitigation in Airborne Passive Radars

Yaqi Deng [1,2,*], Zhengwang Pei [1], Wenguo Li [1,2] and Dongchu Jiang [1,2]

[1] School of Information and Electronic Engineering, Hunan City University, No. 518, Yingbin East Road, Yiyang 413000, China; 18711787833@163.com (Z.P.); liwenguo@hncu.edu.cn (W.L.); dongchujiang@126.com (D.J.)
[2] All-Solid-State Energy Storage Materials and Devices Key Laboratory of Hunan Province, Hunan City University, Yiyang 413000, China
* Correspondence: dengyaqi@hncu.edu.cn

Abstract: In an airborne passive radar, multipath (MP) clutter, which is caused by MP signals contained in the contaminated reference signal, degrades the space-time adaptive processing (STAP) performance. The MP clutter suppression algorithm before STAP can mitigate the influence of impure reference signals. However, the performances of the existing MP clutter suppression methods deteriorate when the intrinsic clutter motion (ICM) exists because the sparse model of MP clutter is disturbed. To eliminate the impacts of ICM on MP clutter suppression, a joint optimization algorithm is developed for airborne passive radar. Firstly, the sparse model of MP clutter is modified by taking ICM fluctuation into account. Subsequently, the joint optimization function of the ICM fluctuation and MP clutter profile is derived. Finally, based on the local search technique, MP clutter is suppressed with ICM error calibration and off-grid effects mitigation. A range of simulations verify the reliability and superiority of the proposed method.

Keywords: intrinsic clutter motion; joint optimization problem; space-time adaptive processing (STAP); airborne passive radar; reference signal

check for updates

Citation: Deng, Y.; Pei, Z.; Li, W.; Jiang, D. Clutter Suppression Algorithm with Joint Intrinsic Clutter Motion Errors Calibration and Off-Grid Effects Mitigation in Airborne Passive Radars. *Appl. Sci.* **2023**, *13*, 5653. https://doi.org/10.3390/app13095653

Academic Editor: Atsushi Mase

Received: 27 March 2023
Revised: 28 April 2023
Accepted: 30 April 2023
Published: 4 May 2023

Copyright: © 2023 by the authors. Licensee MDPI, Basel, Switzerland. This article is an open access article distributed under the terms and conditions of the Creative Commons Attribution (CC BY) license (https://creativecommons.org/licenses/by/4.0/).

1. Introduction

Airborne passive radars exploit the existing transmitters as emitters of opportunity, having attracted widespread attention in recent years [1–7]. Compared with airborne active radars, the lack of dedicated transmitters offers the advantages of low cost, strong survivability, and antijamming. However, the moving airborne platform leading to the received ground clutter is extended in terms of the Doppler frequencies and angle. Thus, it is difficult for a traditional spatial or temporal filter to detect targets.

Space-time adaptive processing (STAP), which uses multichannel spatial information across a sequence of temporal pulses to form a two-dimensional filter, is a crucial technology in airborne passive radar for clutter cancellation. However, the application of STAP is restricted by practical problems, such as excessively high computational complexity and a large number of the required training snapshots. Subsequently, extensive research on STAP mainly considered how to reduce the computational burden and enhance the convergence speed. However, the practical implementation of STAP in airborne passive radar is based on the assumption that the reference signal is uncontaminated. When this condition is not satisfied, the clutter caused by the direct-path (DP) signal (DP clutter) and multipath (MP) signal (MP clutter) affects the covariance matrix estimation. Consequently, the target self-nulling phenomenon may exist [8].

The MP clutter cancellation approach before STAP can eliminate the influence of impure reference signals in airborne passive radars. Existing MP clutter suppression

techniques can be categorized into two groups. One is signal equalization, which relies heavily on precise prior information [9]. Another is the sparse reconstruction of MP clutter that does not require prior knowledge [8,10,11]. However, the pulse-to-pulse fluctuations in MP signals, also known as the intrinsic clutter motion (ICM) [12], degrade the reconstruction quality. Thus, it is a challenge to suppress MP clutter with ICM errors in airborne passive radar systems.

In the current paper, to enhance the MP clutter suppression performance with ICM errors, we present a novel suppression algorithm with ICM error calibration and off-grid effects mitigation. In the proposed algorithm, the ICMs of clutter patches (ICM-CP) and MP scatterers (ICM-MP) are considered. After using reference signals for matched filtering, the DP clutter snapshot involves the temporal fluctuation vector caused by ICM-CP, and the MP clutter snapshot involves the temporal fluctuation vector caused by both ICM-CP and ICM-MP. Consequently, the MP clutter is not only related to the DP clutter snapshot and the modified steering vector, which are mentioned in SRA and LSA, but also related to the ICM-MP fluctuation. Thus, the existing sparse model of MP clutter is disturbed in the presence of ICM-MP. Based on the above analyses, an MP clutter suppression algorithm based on joint optimization is designed. The procedure of the proposed algorithm is described as follows: Initially, the ICM-MP fluctuation is introduced, and the sparse model of MP clutter is revised. Subsequently, by adding a constraint to ICM-MP fluctuation, we modify a traditional reconstruction issue into a joint optimization issue. Thirdly, the ICM-MP fluctuation and MP clutter profile are estimated simultaneously based on the local search technique. Finally, the MP clutter is suppressed with ICM-MP error calibration and off-grid effects mitigation. After the MP clutter cancellation algorithm, the existing STAP is utilized to mitigate the impacts of ICM-DP and cancel DP clutter.

The main contributions of the paper are summarized as follows:

(i) We develop a new sparse model of MP clutter and joint optimization problems by considering ICM-MP fluctuation.
(ii) We propose a joint optimization algorithm for improving the MP clutter suppression performance when ICM-MP fluctuation exists, where the local search technique is incorporated to mitigate off-grid effects.
(iii) The calibration step is efficiently performed, and we discuss the feasibility of the proposed algorithm from practical implementation and computational efficiency perspectives.

The remainder of this paper is organized as follows: We first discuss the related work in Section 2, and the signal model, including ICM for airborne passive radar, is introduced in Section 3. Subsequently, we review the existing optimization problems in SRA and LSA, and then the proposed joint optimization algorithm for MP clutter suppression is derived in Section 4. Section 5 presents some simulated experiments demonstrating the performance and validity of the proposed approach. Finally, Section 6 gives the relevant conclusions.

Notation: In this paper, the Kronecker product and Hadamard product are expressed by the symbols $\otimes$ and $\odot$, respectively. The symbol $E[\cdot]$ indicates the mathematical expectation, and $\mathrm{Re}\{\cdot\}$ represents the real part of the argument. $(\cdot)^T$, $(\cdot)^*$ and $(\cdot)^{\mathrm{H}}$ denotes the transposition, complex conjugation, and conjugate transposition, respectively. $diag(\cdot)$ denotes the diagonal matrix, $\boldsymbol{I}_A$ is the $A \times A$ identity matrix, Toeplitz$(\cdot)$ is the Toeplitz matrix, and $\boldsymbol{1}_{B\times C}$ is the $B \times C$ matrix with all elements being 1. In addition, $\|\cdot\|_F$, $\|\cdot\|_2$ and $\|\cdot\|_1$ represent the Frobenius-norm, l_2-norm, and l_1-norm operations, respectively.

2. Related Work

STAP has been studied extensively in previous works. Initially, the fully adaptive STAP, where adaptive weight is calculated using all elements and pulses, was considered [12,13]. Afterwards, a variety of STAP approaches have been developed to reduce the computational burden and enhance the convergence speed. To improve the detection ability in heterogeneous environments, Mevin et al. proposed a knowledge-aided STAP technique in which the prior information was incorporated within the conventional training

strategies [14]. A similar idea was used in other works [15–18]. The reduced-rank and reduced-dimension STAP, such as subspace projection and extended factored algorithms, have been widely considered since the training requirements were reduced to twice the degrees of freedom or the clutter rank [19–26]. To further reduce the training requirements, Yang et al. proposed the sparse representation STAP [27]. By utilizing intrinsic sparsity and compressive sensing techniques to recover the clutter, estimating the accurate clutter spectrum with minor training support is achievable. Similar conclusions were also obtained in other works [28–32]. The deep learning technique provides a new idea for STAP design. Authors in [33] and [34] used deep convolution networks to offer the high-resolution profile, and simulations demonstrated that deep-learning STAP reduced the computational load compared with sparse representation STAP.

These previous studies for STAP provide some important insights into clutter suppression and target detection for airborne passive radar; however, the common assumption is that the reference signal is pure. In a realistic environment, this assumption is violated. To enable the target detection ability of STAP, the question is how to develop the MP clutter suppression approach before STAP.

In [9], Guo et al. used a blind equalization approach to construct the constraint optimization model and restore the pure DP signal based on the prior information. To overcome the dependence on prior knowledge, some sparse reconstruction algorithms were proposed for MP clutter suppression [8,10,11]. In our previous work [8,10], we derived the sparse reconstruction algorithms (SRAs), in which the sparse model of MP clutter was designed and several optimization algorithms based on the L_1-norm were exploited to estimate the profile. In our previous work [11], under the framework of sparse models in SRAs, we used the local search algorithm (LSA) to select optimal atoms to construct the range-Doppler dictionary and address the off-grid issue. However, the presence of ICM disturbs the sparse model of MP clutter and corrupts the MP clutter suppression performance of SRA and LSA. To the best of our knowledge, very little literature addresses the ICM problem in MP clutter suppression. Although the ICM problem also arose in STAP [35–38], these methods only focused on the DP clutter cancellation. In this paper, we propose a novel MP clutter suppression method to mitigate ICM effects while also taking off-grids into account.

3. Signal Model

The system being considered is an airborne passive radar. We assume that the transmitter is a ground-based non-cooperative emitter and that the airborne platform moves in a straight line with constant altitude H_R and velocity v_R. The side-looking airborne passive radar geometry is shown in Figure 1. The measurement signals are received by a uniform linear array consisting of N elements. The reference antenna is directed toward the non-cooperative transmitter and receives the reference signal. The impure reference signal involves the DP signal, whose time bin is l_{d}, and the N_{T} MP signals, whose time bins are l_p ($p = 1, \ldots, N_T$), respectively. Let the reference signal and measurement signals be segmented uniformly. Then, signals are equivalent to M pulses with a constant pulse repetition interval T_r in a coherent integration time. L is the number of fast-time samples in T_r. After using the segmented signals for matched filtering, the received data set comprises LMN samples. The radar data corresponding to a fast-time sample can be arranged as a $MN \times 1$ space-time snapshot.

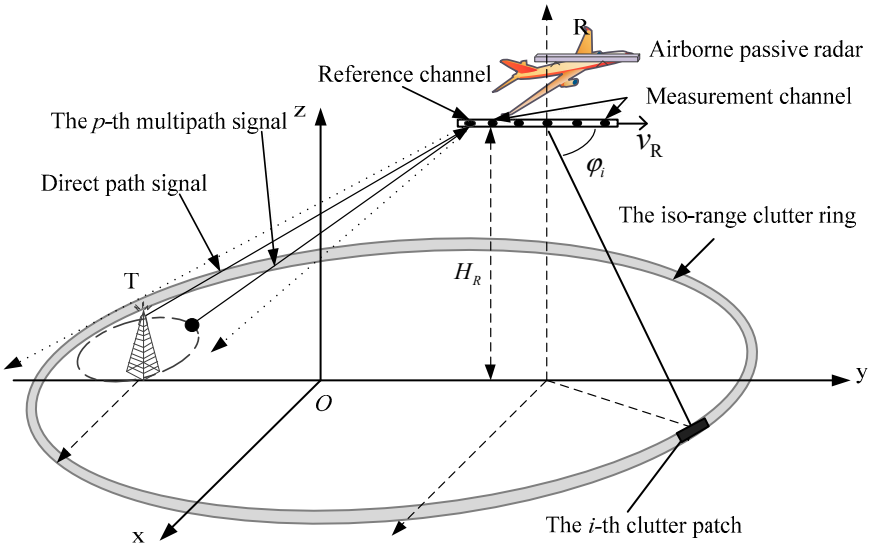


Figure 1. Airborne passive radar geometry.

Considering an impure reference signal and ignoring the influence of range ambiguities, the clutter snapshot at the l-th range cell is composed of two parts. The first part is the DP clutter snapshot, that is, the matched result of the scatterer echoes whose time bin is $(l + l_{\mathrm{d}})$ with the DP signal. The DP clutter space-time snapshot, including ICM-CP, is given by:

$$\boldsymbol{x}_{\mathrm{dc},l} = \sum_{i=1}^{N_c} \xi_{l+l_{\mathrm{d}},i} \boldsymbol{v}_s(\vartheta_i) \otimes (\boldsymbol{v}_t(\omega_i - \omega_{\mathrm{d}}) \odot \boldsymbol{\gamma}_1) = \sum_{i=1}^{N_c} \xi_{l+l_{\mathrm{d}},i} \boldsymbol{T}\boldsymbol{v}(\omega_{\mathrm{d},i}, \vartheta_i), \tag{1}$$

where N_c is the number of statistically independent clutter patches; $\xi_{l+l_{\mathrm{d}},i} = \varepsilon_{l+l_{\mathrm{d}},i}\varepsilon_{\mathrm{d}}^*$, where ε_{d} and $\varepsilon_{l+l_{\mathrm{d}},i}$ are the complex amplitudes of the DP signal and the i-th clutter patch at the $(l + l_d)$-th time bin, respectively; $\vartheta_i = d\cos\varphi_i/\lambda$ and $\omega_i = T_r v_R \cos\varphi_i/\lambda$ are spatial frequency and normalized Doppler frequency of the i-th clutter patch, respectively, where λ is the wavelength, d is the inter-channel spacing, and φ_i is the spatial cone angle of the i-th clutter patch; $\omega_{\mathrm{d},i} = \omega_i - \omega_{\mathrm{d}}$ indicates the relative (relative to the DP signal) normalized Doppler frequency, where $\omega_{\mathrm{d}} = T_r\omega_{\mathrm{d}}{}'$ and $\omega_{\mathrm{d}}{}'$ are the normalized Doppler frequency and Doppler frequency of the DP signal, respectively; $\boldsymbol{\gamma}_1$ is the $M \times 1$ temporal fluctuation vector corresponding to ICM-CP, which leads to the small pulse-to-pulse fluctuations in the scatterer echoes; the ICM-CP fluctuation matrix $\boldsymbol{T} = \boldsymbol{I}_N \otimes diag(\boldsymbol{\gamma}_1)$; $\boldsymbol{v}(\omega, \vartheta) = \boldsymbol{v}_s(\vartheta) \otimes \boldsymbol{v}_t(\omega)$ is the space-time steering vector with

$$\boldsymbol{v}_s(\vartheta) = [1, \exp(j2\pi\vartheta), \cdots, \exp(j2\pi(N-1)\vartheta)]^{\mathrm{T}}, \tag{2}$$

$$\boldsymbol{v}_t(\omega) = [1, \exp(j2\pi\omega), \cdots, \exp(j2\pi(M-1)\omega)]^{\mathrm{T}}, \tag{3}$$

denoting the spatial and temporal steering vectors, respectively.

The second part is the matched result of the scatterer echoes, whose time bin is $(l + l_p)$ $(p = 1, \ldots, N_T)$ with the MP signals, that is, the MP clutter snapshot. In the presence of ICM-CP and ICM-MP, the MP clutter space-time snapshot is given by:

$$\boldsymbol{x}_{pc,l} = \varepsilon_p{}' \sum_{i=1}^{N_c} \xi_{l+l_p,i} \boldsymbol{v}_s(\vartheta_i) \otimes \left(\boldsymbol{v}_t\left(\omega_i - \omega_p\right) \odot \boldsymbol{\gamma}_1 \odot \boldsymbol{\gamma}_2\right) = \varepsilon_p{}' \boldsymbol{\Gamma} \sum_{i=1}^{N_c} \xi_{l+l_p,i} \boldsymbol{T}\boldsymbol{v}\left(\omega_{p,i}, \vartheta_i\right), \tag{4}$$

where $\varepsilon_p{}' = \varepsilon_p^*/\varepsilon_{\mathrm{d}}^*$ represents the relative (relative to the DP signal) amplitude and ε_p is the complex amplitude of the p-th MP signal [8]; $\omega_{p,i} = \omega_i - \omega_p$ is the relative (relative to the p-th MP signal) normalized Doppler frequency, where $\omega_p = T_r\omega_p{}'$ and $\omega_p{}'$ are

the normalized Doppler frequency and Doppler frequency corresponding to the p-th MP signal, respectively; γ_2 is the $M \times 1$ temporal fluctuation vector corresponding to ICM-MP, which means the small pulse-to-pulse fluctuations exist in MP signals; the vector γ_2 is also called the ICM-MP fluctuation vector in what follows; the ICM-MP fluctuation matrix $\mathbf{\Gamma} = \boldsymbol{I}_N \otimes diag(\gamma_2)$.

By defining the modified steering vector $\boldsymbol{f}(\omega_\mathrm{d} - \omega_p) = \boldsymbol{1}_{N\times 1} \otimes \boldsymbol{v}_t(\omega_\mathrm{d} - \omega_p)$, we obtain $\boldsymbol{v}(\omega_{p,i}, \vartheta_i) = \boldsymbol{v}(\omega_{\mathrm{d},i}, \vartheta_i) \odot \boldsymbol{f}(\omega_\mathrm{d} - \omega_p)$. Thus, Equation (4) is reformulated as [8]:

$$\begin{aligned} \boldsymbol{x}_{pc,l} &= \varepsilon_p{}' \mathbf{\Gamma} \boldsymbol{x}_{\mathrm{dc},l+(l_p-l_\mathrm{d})} \odot \boldsymbol{f}(\omega_p - \omega_\mathrm{d}) \\ &= \varepsilon_p{}' \mathbf{\Gamma} \boldsymbol{x}_{l+(l_p-l_\mathrm{d})} \odot \boldsymbol{f}(\omega_p - \omega_\mathrm{d}) - \varepsilon_p{}' \mathbf{\Gamma} \sum_{\overline{p}=1}^{N_T} \varepsilon_{\overline{p}}{}' \mathbf{\Gamma} \boldsymbol{x}_{l+(l_p+l_{\overline{p}}-2l_\mathrm{d})} \odot \boldsymbol{f}(\overline{\omega}_p + \omega_p - 2\omega_\mathrm{d}) \end{aligned} . \tag{5}$$

where the first term and second term of the second equation in Equation (5) are called the true MP clutter and the derived ghost MP clutter, respectively [8]. Thus, the MP clutter snapshot correlates with three parameters, which are the DP clutter snapshot, the ICM-MP fluctuation matrix, and the modified steering vector. Then, the received snapshot at the l-th range cell, consisting of the DP clutter, the MP clutter, and the receiver thermal noise, is expressed as

$$\boldsymbol{x}_l = \boldsymbol{x}_{\mathrm{dc},l} + \sum_{p=1}^{N_T} \boldsymbol{x}_{pc,l} + \boldsymbol{x}_n, \tag{6}$$

where $\boldsymbol{x}_n$ is the noise vector, which is assumed to be spatially and temporally uncorrelated. The complex amplitudes of clutter patches $\xi_{l,i}$, $i = 1, 2, \ldots, N_c$, are assumed to be independent and identically distributed random variables. Hence, the corresponding covariance matrix $\boldsymbol{R}_x$ is given by:

$$\boldsymbol{R}_x = E\left[\boldsymbol{x}_l \boldsymbol{x}_l^\mathrm{H}\right] = \boldsymbol{R}_\mathrm{d} + \sum_{p=1}^{N_T} \boldsymbol{R}_p + \boldsymbol{R}_n, \tag{7}$$

where the DP clutter covariance matrix $\boldsymbol{R}_\mathrm{d} = E\left[\boldsymbol{x}_{\mathrm{dc},l} \boldsymbol{x}_{\mathrm{dc},l}^\mathrm{H}\right]$; the p-th MP clutter covariance matrix $\boldsymbol{R}_p = E\left[\boldsymbol{x}_{pc,l} \boldsymbol{x}_{pc,l}^\mathrm{H}\right]$; $\boldsymbol{R}_n = E\left[\boldsymbol{x}_n \boldsymbol{x}_n^\mathrm{H}\right]$ is the noise covariance matrix.

From the above analyses, it is evident that the presence of MP clutter severely affects the estimated covariance matrix. As a consequence, directly applying the STAP algorithms to suppress interference (DP clutter and MP clutter) requires more degrees of freedom than merely canceling DP clutter [8]. Additionally, the detection performance of STAP degrades seriously when targets fall within the MP clutter area [8].

The MP clutter cancellation method prior to STAP can overcome the influence of contaminated reference signals effectively. However, the presence of ICM-MP fluctuation disturbs the sparse model of MP clutter, and it transforms the reconstruction issue into a joint optimization problem. Consequently, both the existing SRA and LSA suffer from a performance loss in MP clutter estimation, thereby degrading the target detection ability of STAP. As a result, it is significant to devise an MP clutter suppression algorithm with ICM-MP fluctuation mitigation.

4. Proposed MP Clutter Suppression Algorithm Based on Joint Optimization

Here, the existing optimization problem in SRA and LSA is briefly reviewed. Subsequently, the motivations for the proposed joint optimization algorithm are presented, where a constraint to ICM-MP fluctuation is added based on the exiting optimization problem. Finally, the proposed joint optimization method is described.

4.1. Review of the Existing Optimization Problem in SRA and LSA

In the existing SRA and LSA, the MP clutter is related to the DP clutter snapshot and the modified steering vector in the absence of ICM-MP fluctuation. Thus, the whole temporal plane is discretized uniformly into Q grid points. The corresponding normalized

Doppler frequency and modified steering vector are ω_q and $\boldsymbol{f}(\omega_q) = \boldsymbol{1}_{N\times 1} \otimes \boldsymbol{v}_t(\omega_q)$, $q = 1, 2, \ldots, Q$, respectively. Supposing the MP clutter can be expressed by D received snapshots, then the sparse model of MP clutter can be approximated by [8]:

$$\sum_{p=1}^{N_T} \boldsymbol{x}_{pc,l} = \boldsymbol{S}_l \boldsymbol{\alpha}, \tag{8}$$

where the range-Doppler dictionary $\boldsymbol{S}_l = \left[\boldsymbol{S}_{D,l} \odot \boldsymbol{F}_1, \boldsymbol{S}_{D,l} \odot \boldsymbol{F}_2, \ldots, \boldsymbol{S}_{D,l} \odot \boldsymbol{F}_Q\right]$; the $MN \times D$ matrix $\boldsymbol{S}_{D,l} = [\boldsymbol{x}_{l+1}, \boldsymbol{x}_{l+2}, \ldots, \boldsymbol{x}_{l+D}]$, the $MN \times D$ matrix $\boldsymbol{F}_q = 1_{1\times D} \otimes \boldsymbol{f}(\omega_q) = 1_{N\times D} \otimes \boldsymbol{v}_t(\omega_q)$; $\boldsymbol{\alpha}$ indicates the $DQ \times 1$ profile, and there exists a degree of sparsity in $\boldsymbol{\alpha}$ [8].

By denoting $\boldsymbol{S}_{D,n} = \boldsymbol{x}_n \otimes 1_{1\times D}$ and $\boldsymbol{S}_n = \left[\boldsymbol{S}_{D,n} \odot \boldsymbol{F}_1, \boldsymbol{S}_{D,n} \odot \boldsymbol{F}_2, \ldots, \boldsymbol{S}_{D,n} \odot \boldsymbol{F}_Q\right]$, we obtain [8]:

$$\begin{aligned} E\left\{ \left\| \sum_{p=1}^{N_T} \boldsymbol{x}_{pc,l} - \boldsymbol{S}_l \boldsymbol{\alpha} \right\|_2^2 \right\} &= C + E\left\{ \|\boldsymbol{x}_l - \boldsymbol{S}_l \boldsymbol{\alpha}\|_2^2 \right\} + 2\mathrm{Re}\left\{ E\left[\boldsymbol{x}_n^{\mathrm{H}} \boldsymbol{S}_l \boldsymbol{\alpha}\right] \right\} \\ &= C + E\left\{ \|\boldsymbol{x}_l - \boldsymbol{S}_l \boldsymbol{\alpha}\|_2^2 \right\} + 2\mathrm{Re}\left\{ E\left[\boldsymbol{x}_n^{\mathrm{H}} \boldsymbol{S}_n \boldsymbol{\alpha}\right] \right\} \end{aligned}, \tag{9}$$

where $E\left[\boldsymbol{x}_n^{\mathrm{H}} \boldsymbol{S}_n \boldsymbol{\alpha}\right] = E\left[\boldsymbol{x}_n^{\mathrm{H}} diag(\boldsymbol{x}_n) \boldsymbol{\Phi} \boldsymbol{\alpha}\right] = \boldsymbol{\zeta}\boldsymbol{\alpha}$, $\boldsymbol{\zeta} = \sigma^2 1_{1\times MN} \boldsymbol{\Phi}$, the modified steering matrix $\boldsymbol{\Phi} = \left[\boldsymbol{F}_1, \boldsymbol{F}_2, \ldots, \boldsymbol{F}_Q\right]$ and σ^2 is the noise power [8], C is a constant independent of parameters $\boldsymbol{S}_l$ and $\boldsymbol{\alpha}$.

By minimizing the output power, the MP clutter estimation is described as the following optimization problem [8]:

$$\hat{\boldsymbol{\alpha}} = \underset{\boldsymbol{\alpha}}{\mathrm{argmin}} E\left\{ \|\boldsymbol{x}_l - \boldsymbol{S}_l \boldsymbol{\alpha}\|_2^2 \right\} + 2\kappa \|\boldsymbol{\alpha}\|_1 + 2\mathrm{Re}\{\boldsymbol{\zeta}\boldsymbol{\alpha}\}, \tag{10}$$

where κ is a sparse constant parameter.

Based on the above optimization problem, SRA estimates the profile $\boldsymbol{\alpha}$ to suppress MP clutter, and LSA modifies the range-doppler dictionary to overcome the off-grid problem. However, the presence of ICM-MP fluctuations significantly affects the MP clutter suppression performance of SRA and LSA.

4.2. The Motivation of the Proposed Joint Optimization Algorithm

If we define $\boldsymbol{a}_{l_{p,\overline{p}}} = \boldsymbol{\Gamma} \boldsymbol{x}_{l+(l_p+l_{\overline{p}}-2l_\mathrm{d})} \odot \boldsymbol{f}(\overline{\omega}_p + \omega_p - 2\omega_\mathrm{d})$, then the $(p, \overline{p})$-th ghost MP clutter in Equation (5) is $\boldsymbol{x}_{l_{p,\overline{p}}} = \boldsymbol{\Gamma}\left(\varepsilon_p{}' \varepsilon_{\overline{p}}{}' \boldsymbol{a}_{l_{p,\overline{p}}}\right) = \boldsymbol{\Gamma} \boldsymbol{x}'_{l_{p,\overline{p}}}$. Thus, we get [35]:

$$E\left[\boldsymbol{x}_{l_{p,\overline{p}}} \boldsymbol{x}_{l_{p,\overline{p}}}^{\mathrm{H}}\right] - E\left[\boldsymbol{x}'_{l_{p,\overline{p}}} \boldsymbol{x}'^{\mathrm{H}}_{l_{p,\overline{p}}}\right] = \left|\varepsilon_p{}'\right|^2 \left|\varepsilon_{\overline{p}}{}'\right|^2 \left[\tilde{\boldsymbol{\Gamma}} - 1_{MN\times MN}\right] \odot \boldsymbol{R}_a, \tag{11}$$

where $\boldsymbol{R}_a = E\left[\boldsymbol{a}_{l_{p,\overline{p}}} \boldsymbol{a}_{l_{p,\overline{p}}}^{\mathrm{H}}\right]$, $\tilde{\boldsymbol{\Gamma}} = \boldsymbol{I}_{N\times N} \otimes \mathrm{Toeplitz}(\zeta(0), \zeta(1), \ldots, \zeta(M-1))$ and the temporal autocorrelation of the ICM fluctuations is $\zeta(m) = \exp\{-8\pi^2 \sigma_v^2 T_r^2 m^2 / \lambda^2\}$, $m = 0, 1, \ldots, M-1$, λ is wavelength and σ_v is the velocity standard deviation [12]. Since $\left|\varepsilon_p{}'\right|^2 \ll 1$, $\left|\varepsilon_{\overline{p}}{}'\right|^2 \ll 1$ and each element in the matrix $\tilde{\boldsymbol{\Gamma}} - \boldsymbol{1}_{MN\times MN}$ is far less than 1 in general [12], the effect of the covariance matrix $E\left[\boldsymbol{x}_{l_{p,\overline{p}}} \boldsymbol{x}_{l_{p,\overline{p}}}^{\mathrm{H}}\right]$ in STAP can be equivalent to the effect of $E\left[\boldsymbol{x}'_{l_{p,\overline{p}}} \boldsymbol{x}'^{\mathrm{H}}_{l_{p,\overline{p}}}\right]$. Thus, Equation (5) can be approximated by:

$$\boldsymbol{x}_{pc,l} = \varepsilon_p{}' \boldsymbol{\Gamma} \boldsymbol{x}_{l+(l_p-l_\mathrm{d})} \odot \boldsymbol{f}(\omega_p - \omega_\mathrm{d}) - \varepsilon_p{}' \boldsymbol{\Gamma} \sum_{\overline{p}=1}^{N_T} \varepsilon_{\overline{p}}{}' \boldsymbol{x}_{l+(l_p+l_{\overline{p}}-2l_\mathrm{d})} \odot \boldsymbol{f}(\overline{\omega}_p + \omega_p - 2\omega_\mathrm{d}). \tag{12}$$

Therefore, the sparse model of MP clutter in the presence of ICM-MP becomes:

$$\sum_{p=1}^{N_T} \boldsymbol{x}_{pc,l} = \boldsymbol{\Gamma} \boldsymbol{S}_l \boldsymbol{\alpha} = (\boldsymbol{S}_l + \boldsymbol{\Lambda} \boldsymbol{S}_l)\boldsymbol{\alpha}, \tag{13}$$

where $\boldsymbol{\Lambda} = \boldsymbol{\Gamma} - \boldsymbol{I}_{MN} = \boldsymbol{I}_N \otimes diag(\boldsymbol{h})$ and $\boldsymbol{h} = \boldsymbol{\gamma}_2 - \boldsymbol{1}_{M\times 1}$. Here, $\boldsymbol{\Lambda S}_l$ and $\boldsymbol{h}$, which are the functions of the ICM-MP fluctuation vector $\boldsymbol{\gamma}_2$, are defined as the ICM-MP errors calibration matrix and the ICM-MP errors calibration vector, respectively.

Substituting the above equation into Equation (9), we can get:

$$\begin{aligned} E\left\{ \left\| \sum_{p=1}^{N_T} \boldsymbol{x}_{pc,l} - \boldsymbol{\Gamma} \boldsymbol{S}_l \boldsymbol{\alpha} \right\|_2^2 \right\} &= C + E\left\{ \|\boldsymbol{x}_l - \boldsymbol{\Gamma} \boldsymbol{S}_l \boldsymbol{\alpha}\|_2^2 \right\} + 2\mathrm{Re}\left\{ E\left[\boldsymbol{x}_n^{\mathrm{H}} \boldsymbol{\Gamma} \boldsymbol{S}_n \boldsymbol{\alpha} \right] \right\} \\ &= C + E\left\{ \|\boldsymbol{x}_l - \boldsymbol{\Gamma} \boldsymbol{S}_l \boldsymbol{\alpha}\|_2^2 \right\} + 2\mathrm{Re}\left\{ E\left[\boldsymbol{x}_n^{\mathrm{H}} \boldsymbol{\Gamma} diag(\boldsymbol{x}_n) \boldsymbol{\Phi} \boldsymbol{\alpha} \right] \right\} \end{aligned}, \tag{14}$$

where

$$E\left[\boldsymbol{x}_n^{\mathrm{H}} \boldsymbol{\Gamma} diag(\boldsymbol{x}_n) \boldsymbol{\Phi} \boldsymbol{\alpha} \right] = E\left[\boldsymbol{x}_n^{\mathrm{H}} diag(\boldsymbol{x}_n) \right] \boldsymbol{\Gamma} \boldsymbol{\Phi} \boldsymbol{\alpha} = \sigma^2 \boldsymbol{1}_{1\times MN} \boldsymbol{\Gamma} \boldsymbol{\Phi} \boldsymbol{\alpha}. \tag{15}$$

We define $\boldsymbol{\psi} = \sigma^2 \boldsymbol{1}_{1\times MN} \boldsymbol{\Gamma} \boldsymbol{\Phi}$, and we can rewrite the Equation (14) as

$$E\left\{ \left\| \sum_{p=1}^{N_T} \boldsymbol{x}_{pc,l} - \boldsymbol{\Gamma} \boldsymbol{S}_l \boldsymbol{\alpha} \right\|_2^2 \right\} = C + E\left\{ \|\boldsymbol{x}_l - \boldsymbol{\Gamma} \boldsymbol{S}_l \boldsymbol{\alpha}\|_2^2 \right\} + 2\mathrm{Re}\{\boldsymbol{\psi} \boldsymbol{\alpha}\}. \tag{16}$$

By minimizing the ICM-MP error calibration matrix and the output power, the optimization problem can be formulated to estimate the profile vector $\boldsymbol{\alpha}$ and calibration vector $\boldsymbol{h}$ [39]

$$\{\hat{\boldsymbol{\alpha}}, \hat{\boldsymbol{h}}\} = \underset{\boldsymbol{\alpha},\boldsymbol{h}}{\mathrm{argmin}} J(\boldsymbol{\alpha}, \boldsymbol{h}) = \underset{\boldsymbol{\alpha},\boldsymbol{h}}{\mathrm{argmin}} E\left\{ \|\boldsymbol{x}_l - \boldsymbol{\Gamma} \boldsymbol{S}_l \boldsymbol{\alpha}\|_2^2 \right\} + 2\kappa \|\boldsymbol{\alpha}\|_1 + 2\mathrm{Re}\{\boldsymbol{\psi} \boldsymbol{\alpha}\} + \|\boldsymbol{\Lambda} \boldsymbol{S}_l\|_F^2, \tag{17}$$

where $\boldsymbol{\Gamma} = \boldsymbol{I}_N \otimes diag(\boldsymbol{1}_{M\times 1} + \boldsymbol{h})$.

Based on the above analyses, the MP clutter suppression problem is equivalent to the estimation problem of the profile vector $\boldsymbol{\alpha}$ and calibration vector $\boldsymbol{h}$. To overcome this issue, the calibration vector $\boldsymbol{h}$ must first be fixed. Thus, the minimization of Equation (17) with a profile $\boldsymbol{\alpha}$ becomes:

$$J_1(\boldsymbol{\alpha}) = E\left\{ \|\boldsymbol{x}_l - \boldsymbol{\Gamma} \boldsymbol{S}_l \boldsymbol{\alpha}\|_2^2 \right\} + 2\kappa \|\boldsymbol{\alpha}\|_1 + 2\mathrm{Re}\{\boldsymbol{\psi} \boldsymbol{\alpha}\}. \tag{18}$$

We compute the gradient terms of the above equation with respect to $\boldsymbol{\alpha}^*$, and let the gradient terms equal zero. Thus, we get:

$$\boldsymbol{\alpha} = \boldsymbol{R}_S^{-1} \left(\boldsymbol{r}_{Sx} - \kappa \mathrm{sign}(\boldsymbol{\alpha}) + \boldsymbol{\psi}^{\mathrm{H}} \right), \tag{19}$$

where $\boldsymbol{R}_S = E\left[\boldsymbol{S}_l^{\mathrm{H}} \boldsymbol{\Gamma}^{\mathrm{H}} \boldsymbol{\Gamma} \boldsymbol{S}_l \right]$; $\boldsymbol{r}_{Sx} = E\left[\boldsymbol{S}_l^{\mathrm{H}} \boldsymbol{\Gamma}^{\mathrm{H}} \boldsymbol{x}_l \right]$ and $\mathrm{sign}(\cdot)$ denotes a component-wise function.

On the other hand, by fixing the profile vector $\boldsymbol{\alpha}$, the estimation of $\boldsymbol{h}$ is transformed into the following optimization problem:

$$J_2(\boldsymbol{h}) = E\left\{ \|\boldsymbol{x}_l - \boldsymbol{\Gamma} \boldsymbol{S}_l \boldsymbol{\alpha}\|_2^2 \right\} + 2\mathrm{Re}\{\boldsymbol{\psi} \boldsymbol{\alpha}\} + \|\boldsymbol{\Lambda} \boldsymbol{S}_l\|_F^2. \tag{20}$$

Since $\boldsymbol{\Lambda} = \boldsymbol{I}_N \otimes diag(\boldsymbol{h})$ and $\boldsymbol{\Gamma} = \boldsymbol{I}_N \otimes diag(\boldsymbol{1}_{M\times 1} + \boldsymbol{h})$ are the diagonal matrices, we get $\|\boldsymbol{\Lambda}\boldsymbol{S}_l\|_F^2 = C_1\|\boldsymbol{\Lambda}\|_F^2 = C_1 N\|\boldsymbol{h}\|_2^2$ where C_1 is a constant, and

$$\begin{aligned} \mathrm{Re}\{\boldsymbol{\psi}\boldsymbol{\alpha}\} &= \mathrm{Re}\{\sigma^2 \boldsymbol{1}_{1\times MN}[\boldsymbol{I}_N \otimes diag(\boldsymbol{1}_{M\times 1} + \boldsymbol{h})]\boldsymbol{\Phi}\boldsymbol{\alpha}\} \\ &= \mathrm{Re}\{\sigma^2 \boldsymbol{1}_{1\times MN}\boldsymbol{\Phi}\boldsymbol{\alpha}\} + \mathrm{Re}\{\sigma^2 \boldsymbol{1}_{1\times MN}[\boldsymbol{I}_N \otimes diag(\boldsymbol{h})]\boldsymbol{\Phi}\boldsymbol{\alpha}\} \\ &= C_2 + \mathrm{Re}\Big\{\sigma^2 (\boldsymbol{\Phi}\boldsymbol{\alpha})^T (\boldsymbol{1}_{N\times 1} \otimes \boldsymbol{I}_M)\boldsymbol{h}\Big\} \end{aligned}. \tag{21}$$

For simplicity, we denote $\boldsymbol{\varsigma} = \sigma^2 (\boldsymbol{\Phi}\boldsymbol{\alpha})^T (\boldsymbol{1}_{N\times 1} \otimes \boldsymbol{I}_M)$. Then, Equation (20) can be reformulated as:

$$\begin{aligned} J_2(\boldsymbol{h}) &= E\Big\{\|\boldsymbol{x}_l - \boldsymbol{S}_l\boldsymbol{\alpha} - [\boldsymbol{I}_N \otimes diag(\boldsymbol{h})]\boldsymbol{S}_l\boldsymbol{\alpha}\|_2^2\Big\} + 2\mathrm{Re}\{\boldsymbol{\varsigma}\boldsymbol{h}\} + \|\boldsymbol{h}\|_2^2 \\ &= E\Big\{\|\boldsymbol{e}_l - \boldsymbol{G}_l\boldsymbol{h}\|_2^2\Big\} + 2\mathrm{Re}\{\boldsymbol{\varsigma}\boldsymbol{h}\} + \|\boldsymbol{h}\|_2^2 \end{aligned}, \tag{22}$$

where $\boldsymbol{e}_l = \boldsymbol{x}_l - \boldsymbol{S}_l\boldsymbol{\alpha}$ and $\boldsymbol{G}_l = diag(\boldsymbol{S}_l\boldsymbol{\alpha})(\boldsymbol{1}_{N\times 1} \otimes \boldsymbol{I}_M)$. We obtain the gradient terms of Equation (22) with respect to the calibration vector:

$$\nabla J_h = \frac{\partial J_2(\boldsymbol{h})}{\partial \boldsymbol{h}^*} = \boldsymbol{R}_G\boldsymbol{h} - \boldsymbol{r}_{Ge} + \boldsymbol{\varsigma}^{\mathrm{H}}, \tag{23}$$

where $\boldsymbol{R}_G = E\Big[\boldsymbol{G}_l^{\mathrm{H}}\boldsymbol{G}_l\Big] + \boldsymbol{I}_M$ and $\boldsymbol{r}_{Ge} = E\Big[\boldsymbol{G}_l^{\mathrm{H}}\boldsymbol{e}_l\Big]$. Let the above equation be equal to zero, and then we get:

$$\boldsymbol{h} = \boldsymbol{R}_G^{-1}\Big(\boldsymbol{r}_{Ge} - \boldsymbol{\varsigma}^{\mathrm{H}}\Big). \tag{24}$$

Now, expressions (19) and (24), derived from the optimization problem presented in Equation (17), are obtained to estimate the profile vector $\boldsymbol{\alpha}$ and the calibration vector $\boldsymbol{h}$. However, it is difficult to obtain the analytical solutions of $\boldsymbol{\alpha}$ and $\boldsymbol{h}$ by directly solving these two expressions. This is because Equations (19) and (24) are not closed-form expressions for $\boldsymbol{\alpha}$ and $\boldsymbol{h}$, that is, the variables $\boldsymbol{R}_S$, $\boldsymbol{r}_{Sx}$ and $\boldsymbol{\psi}$ in Equation (19) are functions of $\boldsymbol{h}$, and the variables $\boldsymbol{R}_G$, $\boldsymbol{r}_{Ge}$ and $\boldsymbol{\varsigma}$ in Equation (24) are functions of $\boldsymbol{\alpha}$. Therefore, estimating the vectors $\boldsymbol{\alpha}$ and $\boldsymbol{h}$ jointly provides an alternative solution.

The above development shows that the ICM-MP fluctuation vector/matrix affects the existing sparse model of MP clutter and optimization problems. Consequently, the MP clutter suppression performance is degraded in SRA and LSA, which will be presented in Section 5. On the other hand, it is concluded from reference [11] that off-grid issues are difficult to avoid in practice. Thus, it is necessary to develop a joint optimization algorithm with fluctuation error calibration and off-grid effect mitigation.

4.3. The Proposed Joint Optimization Algorithm

Here, the joint optimization algorithm for the ICM-MP fluctuation and profile estimation is derived. Subsequently, a two-step suppression method for MP clutter and DP clutter cancellation is presented, and the overall procedure of the proposed joint optimization algorithm is summarized.

In the joint optimization algorithm, two steps are performed in each external alternation: (a) the profile estimation step, where the local search technique presented in reference [11] is exploited to mitigate off-grid effects; and (b) the ICM-MP errors calibration step, where the calibration vector $\boldsymbol{h}$ is estimated.

In the profile estimation step of the k-th external alternation, the profile vector $\boldsymbol{\alpha}$ is estimated with off-grid effect mitigation. In each external alternation, the optimal atoms representing MP clutter are selected by several iterative searches [11]. Each iterative search contains a global search and several local searches, and an optimal atom is determined when each iterative search is completed. For simplicity, let symbol (k, m) denote the m-th ($m = 1, 2, 3, \cdots$) iterative search in the k-th external alternation, and let symbols $(k, m, 0)$

and $(k,m,n)(n=1,2,\ldots)$ be the global search and the n-th local search of the (k,m)-th iterative search, respectively.

Initially, we discretize the temporal plane with a relatively large interval $\Delta\omega$, and build the following range-Doppler dictionary, termed the global dictionary.

$$\begin{aligned}\boldsymbol{S}_l &= \left[\boldsymbol{x}_{l+1}\odot\boldsymbol{f}(\omega_1),\ldots,\boldsymbol{x}_{l+D}\odot\boldsymbol{f}(\omega_1),\ldots,\boldsymbol{x}_{l+1}\odot\boldsymbol{f}(\omega_Q),\ldots,\boldsymbol{x}_{l+D}\odot\boldsymbol{f}(\omega_Q)\right]\\ &= \left[\boldsymbol{g}_{l,1},\cdots,\boldsymbol{g}_{l,D},\cdots,\boldsymbol{g}_{l,(Q-1)D+1},\cdots,\boldsymbol{g}_{l,DQ}\right]\end{aligned}, \tag{25}$$

where $\boldsymbol{g}_{l,\eta}$ $(\eta=1,2,\ldots,DQ)$ is the η-th global atom. Then, the global index in the $(k,m,0)$-th global search is picked up by [11]:

$$\eta(k,m,0)=\arg\max_{\eta\in\{1,2,\ldots,DQ\}} E\left[\boldsymbol{g}_{l,\eta}^{\mathrm{H}}\hat{\boldsymbol{\Gamma}}^{\mathrm{H}}(k-1)\hat{\boldsymbol{e}}_l'(k,m)\right], \tag{26}$$

where $\hat{\boldsymbol{e}}_l'(k,m)$ is the residual vector, which is initialized as $\hat{\boldsymbol{e}}_l'(k,1)=\boldsymbol{x}_l$. Based on the selected global index, the range cell and normalized Doppler frequency corresponding to the optimal global atom $\boldsymbol{g}_{l,\eta(k,m,0)}$ are denoted by $\hat{\tau}(k,m)$ and $\omega(k,m,0)$, respectively.

Subsequently, we conducted several local searches. Motivated by the local search technique [11], the local dictionary in the (k,m,n)-th local search is expressed as:

$$\begin{aligned}\boldsymbol{S}_l(k,m,n) &= \left[\boldsymbol{x}_{l+\hat{\tau}(k,m)}\odot\boldsymbol{f}\left(\omega(k,m,n-1)-\tfrac{\Delta\omega}{2^n}\right),\boldsymbol{x}_{l+\hat{\tau}(k,m)}\odot\boldsymbol{f}(\omega(k,m,n-1)),\boldsymbol{x}_{l+\hat{\tau}(k,m)}\odot\boldsymbol{f}\left(\omega(k,m,n-1)+\tfrac{\Delta\omega}{2^n}\right)\right]\\ &= \left[\boldsymbol{g}_{l,1}(k,m,n),\boldsymbol{g}_{l,2}(k,m,n),\boldsymbol{g}_{l,3}(k,m,n)\right]\end{aligned}. \tag{27}$$

Correspondingly, the local index in the (k,m,n)-th local search is [11]:

$$\eta(k,m,n)=\arg\max_{\eta\in\{1,2,3\}} a_\eta(k,m,n)=\arg\max_{\eta\in\{1,2,3\}} E\left[\boldsymbol{g}_{l,\eta}^{\mathrm{H}}(k,m,n)\hat{\boldsymbol{\Gamma}}^{\mathrm{H}}(k-1)\hat{\boldsymbol{e}}_l'(k,m)\right], \tag{28}$$

where $a_\eta(k,m,n)$ denotes the local response. Thus, the optimal local atom is $\boldsymbol{g}_{l,\eta(k,m,n)}$ and the corresponding normalized Doppler frequency is $\omega(k,m,n)$.

When $\max\{a_\eta(k,m,n)-a_\eta(k,m,n-1)\}$ is less than the local threshold δ_1, the local search terminates, which also means the (k,m)-th iterative search has been completed and an optimal atom is determined. Supposing the optimal normalized Doppler frequency is $\hat{\omega}(k,m)$, then the optimal atom is $\hat{\boldsymbol{g}}_l(k_m)=\boldsymbol{x}_{l+\hat{\tau}(k,m)}\odot\boldsymbol{f}(\hat{\omega}(k,m))$. Let $\hat{\boldsymbol{S}}_l$ and $\hat{\boldsymbol{\Phi}}$ be the optimal dictionary and modified steering matrix, respectively. $\hat{\boldsymbol{S}}_l$ and $\hat{\boldsymbol{\Phi}}$ are initialized as $\hat{\boldsymbol{S}}_l(k,0)=\varnothing$ and $\hat{\boldsymbol{\Phi}}_l(k,0)=\varnothing$, and updated by $\hat{\boldsymbol{S}}_l(k,m)=\left[\hat{\boldsymbol{S}}_l(k,m-1),\hat{\boldsymbol{g}}_l(k,m)\right]$ and $\hat{\boldsymbol{\Phi}}(k,m)=\left[\hat{\boldsymbol{\Phi}}(k,m-1),\boldsymbol{f}(\hat{\omega}(k,m))\right]$, respectively. Therefore, based on Equation (19), the profile vector $\boldsymbol{\alpha}$ at the (k,m)-th iterative search is calculated by using $\hat{\boldsymbol{\Gamma}}(k-1)$.

$$\hat{\boldsymbol{\alpha}}(k,m)=\hat{\boldsymbol{R}}_S^{-1}(k,m)\left(\hat{\boldsymbol{r}}_{Sx}(k,m)+\hat{\boldsymbol{\psi}}^{\mathrm{H}}(k,m)\right), \tag{29}$$

where $\hat{\boldsymbol{R}}_S(k,m)=E\left[\hat{\boldsymbol{S}}_l^{\mathrm{H}}(k,m)\hat{\boldsymbol{\Gamma}}^{\mathrm{H}}(k-1)\hat{\boldsymbol{\Gamma}}(k-1)\hat{\boldsymbol{S}}_l(k,m)\right]$; $\hat{\boldsymbol{r}}_{Sx}(k,m)=E\left[\hat{\boldsymbol{S}}_l^{\mathrm{H}}(k,m)\hat{\boldsymbol{\Gamma}}^{\mathrm{H}}(k-1)\boldsymbol{x}_l\right]$ and $\hat{\boldsymbol{\psi}}(k,m)=\sigma^2\boldsymbol{1}_{1\times MN}\hat{\boldsymbol{\Gamma}}(k-1)\hat{\boldsymbol{\Phi}}(k,m)$. Correspondingly, the residual vector is updated by $\hat{\boldsymbol{e}}_l'(k,m+1)=\boldsymbol{x}_l-\hat{\boldsymbol{\Gamma}}(k-1)\hat{\boldsymbol{S}}_l(k,m)\hat{\boldsymbol{\alpha}}(k,m)$.

The iterative search terminates until $I(k,m)-I(k,m-1)$ is smaller than the search threshold δ_2, where $I(k,m)=SINR(k,m)/SNR_{\mathrm{opt}}$ denotes the signal-to-interference-plus-noise-ratio (SINR) loss of the (k,m)-th iterative search, $SINR(k,m)$ and SNR_{opt} are SINR of the (k,m)-th iterative search and the optimum output signal-to-noise ratio in an interference-free environment, respectively [12]. It also means the profile estimation step of the k-th external alternation has been completed, and all optimal atoms representing MP clutter have been selected. Consequently, we obtain the profile vector $\hat{\boldsymbol{\alpha}}(k)$ in the k-th external alternation. The corresponding optimal dictionary and modified steering matrix are expressed as $\hat{\boldsymbol{S}}_l(k)$ and $\hat{\boldsymbol{\Phi}}(k)$, respectively.

In the ICM-MP error calibration step of the k-th external alternation, the calibration vector $\boldsymbol{h}$ is calculated based on Equation (24)

$$\hat{\boldsymbol{h}}(k) = \hat{\boldsymbol{R}}_G^{-1}(k)\left(\hat{\boldsymbol{r}}_{Ge}(k) - \hat{\boldsymbol{\varsigma}}^{\mathrm{H}}(k)\right), \tag{30}$$

where the covariance matrix $\hat{\boldsymbol{R}}_G(k) = E\left[\hat{\boldsymbol{G}}_l^{\mathrm{H}}(k)\hat{\boldsymbol{G}}_l(k) + \boldsymbol{I}_M\right]$; the cross-correlation vector $\hat{\boldsymbol{r}}_{Ge}(k) = E\left[\hat{\boldsymbol{G}}_l^{\mathrm{H}}(k)\hat{\boldsymbol{e}}_l(k)\right]$; $\hat{\boldsymbol{e}}_l(k) = \boldsymbol{x}_l - \hat{\boldsymbol{S}}_l(k)\hat{\boldsymbol{\alpha}}(k)$ and $\hat{\boldsymbol{G}}_l(k) = diag\left(\hat{\boldsymbol{S}}_l(k)\hat{\boldsymbol{\alpha}}(k)\right)(\boldsymbol{1}_{N\times 1} \otimes \boldsymbol{I}_M)$; and $\hat{\boldsymbol{\varsigma}}(k) = \sigma^2\left(\hat{\boldsymbol{\Phi}}(k)\hat{\boldsymbol{\alpha}}(k)\right)^T(\boldsymbol{1}_{N\times 1} \otimes \boldsymbol{I}_M)$.

To efficiently estimate $\hat{\boldsymbol{h}}(k)$, let

$$\begin{aligned}\hat{\boldsymbol{B}}(k) &= \mathrm{diag}\left(\hat{\boldsymbol{S}}_l^*(k)\hat{\boldsymbol{\alpha}}^*(k)\right)\mathrm{diag}\left(\hat{\boldsymbol{S}}_l(k)\hat{\boldsymbol{\alpha}}(k)\right) \\ &= \mathrm{diag}\left[\hat{\boldsymbol{b}}_1(k), \hat{\boldsymbol{b}}_2(k), \cdots, \hat{\boldsymbol{b}}_N(k)\right]\end{aligned}, \tag{31}$$

where the $1 \times M$ vector $\hat{\boldsymbol{b}}_i(k)$ is composed of $((i-1)M+1)$-th to (iM)-th diagonal elements of $\hat{\boldsymbol{B}}(k)$. Then, we get:

$$\begin{aligned}\hat{\boldsymbol{G}}_l^{\mathrm{H}}(k)\hat{\boldsymbol{G}}_l(k) &= (\boldsymbol{1}_{1\times N} \otimes \boldsymbol{I}_M)\hat{\boldsymbol{B}}(k)(1_{N\times 1} \otimes \boldsymbol{I}_M) \\ &= \left[\mathrm{diag}\left(\hat{\boldsymbol{b}}_1(k)\right), \mathrm{diag}\left(\hat{\boldsymbol{b}}_2(k)\right), \cdots, \mathrm{diag}\left(\hat{\boldsymbol{b}}_N(k)\right)\right]\left[\boldsymbol{I}_M, \boldsymbol{I}_M, \cdots, \boldsymbol{I}_M\right]^T \\ &= \mathrm{diag}\left(\sum_{i=1}^{N}\hat{\boldsymbol{b}}_i(k)\right)\end{aligned}. \tag{32}$$

Thus, $\hat{\boldsymbol{G}}_l^{\mathrm{H}}(k)\hat{\boldsymbol{G}}_l(k)$ is the diagonal matrix, and the diagonal matrix $\hat{\boldsymbol{R}}_G(k) = diag\left(\left[\hat{R}_{k,1}, \hat{R}_{k,2}, \ldots, \hat{R}_{k,M}\right]\right)$. Then, Equation (30) is efficiently calculated by:

$$\hat{\boldsymbol{h}}(k) = \left[\hat{r}_{k,1}/\hat{R}_{k,1}, \hat{r}_{k,2}/\hat{R}_{k,2}, \ldots, \hat{r}_{k,M}/\hat{R}_{k,M}\right]^T, \tag{33}$$

where $\hat{r}_{k,i}$ is the i-th element of $\hat{\boldsymbol{r}}_{Ge}(k) - \hat{\boldsymbol{\varsigma}}^{\mathrm{H}}(k)$. Correspondingly, the update of the ICM-MP fluctuation matrix is given by $\hat{\boldsymbol{\Gamma}}(k) = \boldsymbol{I}_N \otimes diag\left(\boldsymbol{1}_{M\times 1} + \hat{\boldsymbol{h}}(k)\right)$.

When the gain of the cost function expressed by Equation (17) is less than a predetermined alternation threshold δ_3 [39], the alternating step between Equations (29) and (33) terminates.

A summary of the proposed joint optimization algorithm is presented in Figure 2.

After obtaining the profile vector and the calibration vector, a two-step suppression process is performed. First, the MP clutter is canceled by utilizing the proposed joint optimization algorithm. By exploiting the estimated $\hat{\boldsymbol{\alpha}}$ and $\hat{\boldsymbol{h}}$, the output at the l-th range cell is:

$$\boldsymbol{y}_l = \boldsymbol{x}_l - \hat{\boldsymbol{\Gamma}}\hat{\boldsymbol{S}}_l\hat{\boldsymbol{\alpha}}. \tag{34}$$

Then, the STAP algorithm is used for DP clutter cancellation. Supposing the estimated ICM-CP fluctuation matrix $\hat{\boldsymbol{T}}$ is obtained by prior knowledge or the alternating direction method [40], then the snapshot after MP clutter suppression and ICM-CP calibration can be expressed as $\boldsymbol{y}_l' = \hat{\boldsymbol{T}}^{-1}\boldsymbol{y}_l = \hat{\boldsymbol{T}}^{-1}\left(\boldsymbol{x}_l - \hat{\boldsymbol{\Gamma}}\hat{\boldsymbol{S}}_l\hat{\boldsymbol{\alpha}}\right)$. The STAP weight vector is calculated by:

$$\boldsymbol{w}_{y'} = \frac{\hat{\boldsymbol{R}}_u^{-1}\boldsymbol{v}(\varpi_t, \vartheta_t)}{\boldsymbol{v}^{\mathrm{H}}(\varpi_t, \vartheta_t)\hat{\boldsymbol{R}}_u^{-1}\boldsymbol{v}(\varpi_t, \vartheta_t)}, \tag{35}$$

where $\hat{\boldsymbol{R}}_u = 1/K\sum_{k=1,k\neq l}^{K+1}\boldsymbol{y}'_k\boldsymbol{y}'^{\mathrm{H}}_k$ and $\boldsymbol{v}(\varpi_t, \vartheta_t)$ is the space-time vector of the hypothetic target. Then, the scalar output is:

$$z_l = \boldsymbol{w}_{y'}^{\mathrm{H}}\boldsymbol{y}_l' = \boldsymbol{w}_{y'}^{\mathrm{H}}\hat{\boldsymbol{T}}^{-1}\left(\boldsymbol{x}_l - \hat{\boldsymbol{\Gamma}}\hat{\boldsymbol{S}}_l\hat{\boldsymbol{\alpha}}\right). \tag{36}$$

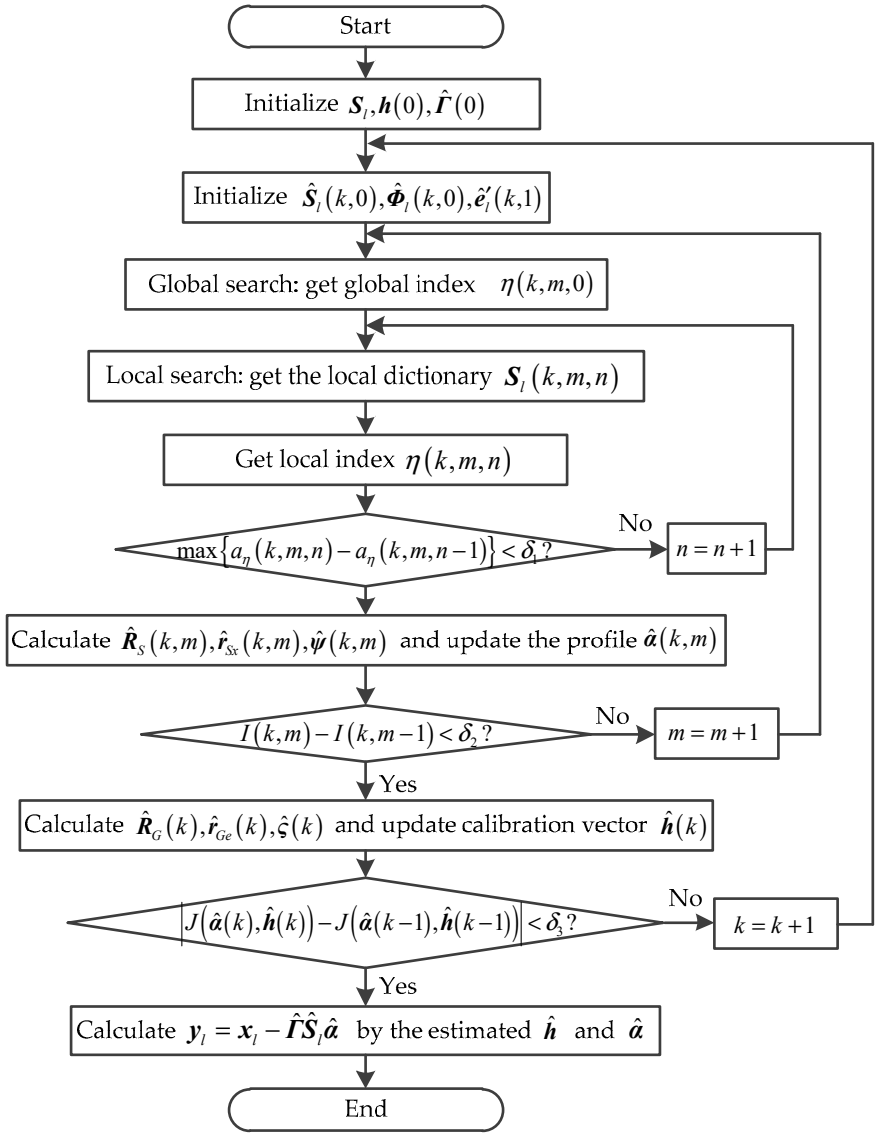


Figure 2. Flow chart of the proposed joint optimization algorithm.

4.4. Analyses of Computational Complexity

In this subsection, we discuss the computational complexity of the proposed algorithm in terms of the number of additions and multiplications. In the k-th external alternation, $(L_2+1)MNDQ$ multiplications and $L_2DQ(MN-1)$ additions are required to compute $\eta(k,m,0)$ in global search, where L_2 denotes the number of samples used to compute mathematical expectation, $3MNK_n(L_2+2)$ multiplications and $3L_2K_n(MN-1)$ additions are required to compute $\eta(k,m,n)$ in local search, where K_n is the local search number, $o(m^3) + m^2(MNL_2+1) + MN(3mL_2+m+1)$ multiplications and $o(m^3) + m^2(MNL_2 - L_2 + 1) + m(MN-1)(L_2+1)$ additions are required to compute $\hat{\boldsymbol{\alpha}}(k,m)$, $2mMN$ multiplications and mMN additions are required to compute $\hat{\boldsymbol{e}}_l'(k,m)$. Thus, in the step of updating $\hat{\boldsymbol{\alpha}}$, $\sum_{m=N_1-N_2-1}^{N_1}\left[o(m^3) + m^2 + MN\left(m^2L_2 + 3mL_2 + 3m + 1\right)\right] + N_2MN(L_2DQ + 3L_2K_n + DQ + 6K_n)$ multiplications and $N_2L_2(MN-1)(3K_n+DQ) + \sum_{m=N_1-N_2-1}^{N_1}\left[o(m^3) + L_2(MN-1)(m^2+m) + m(m+2MN-1)\right]$ additions are required, where N_1 is the iterative search number, and N_2 is the number of updating $\hat{\mathbf{S}}_l(k,m)$. In the step of updating $\hat{\boldsymbol{h}}$, $L_2MN(N_1+1)$ multiplications and $L_2M(NN_1-1)+M$ additions are required to compute $\hat{\mathbf{R}}_G(k)$, $L_2MN(2M+1)$ multiplications and $L_2M(2MN+N-2)$

additions are required to compute $\hat{\boldsymbol{r}}_{Ge}(k)$, and $M + MN(M + N_1)$ multiplications and $MN(M + N_1 - 1)$ additions are required to compute $\hat{\boldsymbol{h}}(k)$. Thus, $L_2MN(2M + N_1 + 2) + M + MN(M + N_1)$ multiplications and $L_2M(2MN + NN_1 + N - 3) + M + MN(M + N_1 - 1)$ additions are required. From the above analyses, the added ICM-MP error calibration step slightly increases the computational cost of the proposed algorithm.

5. Simulations and Performance Analyses

In this section, some examples with simulated data are used to verify the suppression performance of the proposed joint optimization algorithm. In the simulation, the transmitted digital video broadcasting signal is approximated by the Gaussian random signal [8]. The important parameters of the simulated scenarios are given in Table 1. The reference channel receives the DP signal and three MP signals. The normalized Doppler frequency of the DP signal is 0.5, and the DP signal to noise ratio is set to 60 dB where the noise power is normalized. The relative (relative to DP signal) time bins-relative (relative to DP signal) normalized Doppler frequencies-MP signal to DP signal ratios (MDRs) of three MP signals are (3, 0.23, −18 dB), (4, −0.08, −18 dB), and (9, −0.22, −25 dB), respectively. The velocity standard deviations of ICM-CP fluctuation and ICM-MP fluctuation are $\sigma_{1,v} = 0.5$ and $\sigma_{2,v} = 0.7$, respectively. A total of 20 training samples are used in global and local searches to select atoms. Further, 200 training samples are used to estimate the covariance matrix. In addition, we set $Q = 11$, local threshold $\delta_1 = 0.00001$ and a search threshold $\delta_2 = 0.1$ for the proposed joint optimization algorithm.

Table 1. Simulation parameters of an airborne passive radar system.

Parameter	Value
Number of spatial elements	10
Number of temporal pulses	10
Antenna array	Side-looking array
inter-channel spacing	$\lambda/2$
Pulse repetition interval	2.5 ms
Platform velocity	100 m/s
Number of clutter patches in each range cell	181
Range cell index of target	1000
Normalized Doppler frequency of target	−0.28
Signal-to-noise ratio of target	0 dB

5.1. Selection of the Number of Snapshots D

First, we present the SINR loss performance of the proposed joint optimization algorithm versus the number of snapshots in the range-Doppler dictionary (the value of D). Figure 3 gives the simulation results. It is seen that the SINR loss performance depends on the value of D. As D increases, more atoms are used to construct a global dictionary and match MP clutter. Hence, the MP clutter estimation error is decreased and the SINR loss performance is enhanced. On the other hand, an increasing dimension in the range-Doppler dictionary leads to higher computational complexity. Therefore, the value of D is selected by making a trade-off between the computational cost and SINR loss performance. Based on the experimental results, D is set at 9.

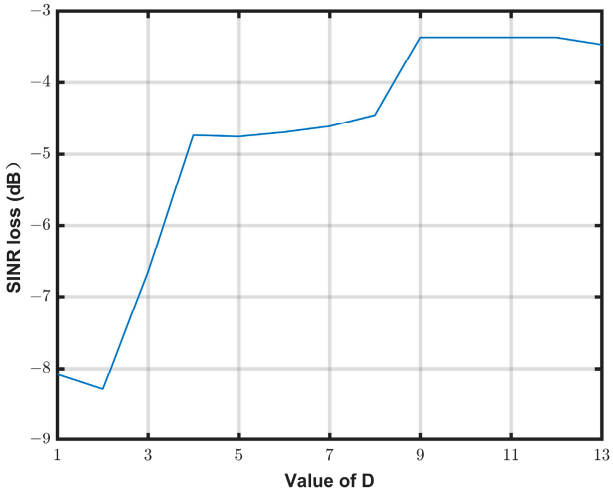


Figure 3. SINR loss performance of the proposed approach versus the value of D.

5.2. Setting of the Alternation Threshold δ_3

Figure 4 gives the gain in performance in the cost function versus the external alternation number in the proposed method. It is seen that the gain in cost function tends to zero gradually with the increasing number of external alternations, which means the profile estimation and the ICM-MP error calibration are close to steady-state performance. However, the value of the cost function will not improve much when the external alternation number is too large and the computational load is heavy. Thus, for this reason and to keep the complexity low, we adopt $\delta_3 = 0.1$ in the following experiments. In Figure 4, the alternation threshold is expressed as the red horizontal line. As a result, the number of external alternations equals eight.

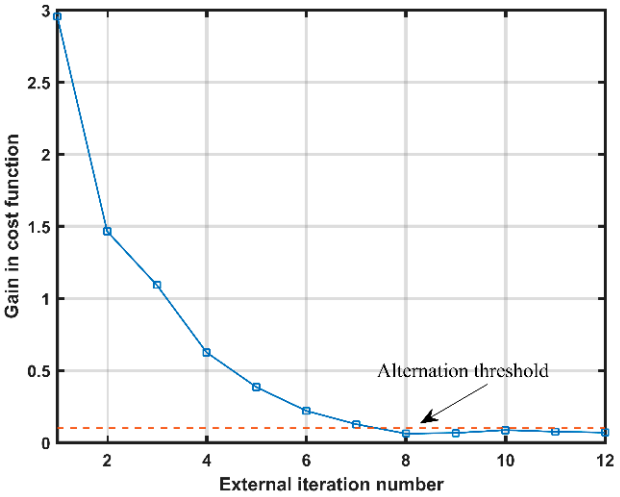


Figure 4. Gain performance in cost function versus external alternation number.

5.3. Comparison with the Exiting Methods

In the third experiment, ICM-CP and ICM-MP are considered, and we compare the performances of the proposed algorithm with those of the existing others, i.e., STAP, LSA, and SRA. In STAP, the existing STAP algorithm is used to suppress DP and MP clutter simultaneously with the ICM-CP mitigation. For a fair and reasonable comparison, LSA, SRA, and the proposed algorithm use the same STAP algorithm to remove DP clutter. In the existing LSA and SRA, we separate the temporal plane into 11 cells, and $D = 9$. For SRA, the forgetting factor is set to 0.95 and the constraint parameter is 70. For LSA, we set

the local threshold at 0.0001 and the iteration threshold at 0.1, which are the same as the local threshold and search threshold in the proposed algorithm, respectively.

First, the distributions of optimal atoms selected by the proposed joint optimization algorithm and LSA are discussed. Table 2 gives the range-Doppler results of the selected atoms for different methods. The atoms corresponding to the real MP clutter component are called as real atoms, and the range-Doppler parameters of real atoms are also presented in Table 2. In the simulation, the number of iterative searches in LSA and the proposed algorithm are both six. Based on the simulated MDRs of three MP signals, the six real atoms are composed of three true atoms and three ghost atoms. Based on Equation (5), the range-Doppler parameters of a true atom and a ghost atom are denoted by $\left[l_p - l_{\mathrm{d}}, \omega_p - \omega_{\mathrm{d}}\right]$ and $\left[l_p + l_{\overline{p}} - 2l_{\mathrm{d}}, \overline{\omega}_p + \omega_p - 2\omega_{\mathrm{d}}\right]$, respectively. As can be seen from Table 2, the selected atoms of LSA, especially the sixth selected atom, deviate far from the real atoms. This is because the presence of ICM-MP fluctuations affects the sparse model and disturbs the selection criteria. Compared with LSA, the selected atoms in the proposed algorithm are closer to the real atoms owing to the added ICM-MP error calibration step. This also indicates that the proposed algorithm can eliminate the impact of ICM-MP fluctuation on local search techniques, providing an accurate estimation for the MP clutter profile.

Table 2. Range-Doppler results of selected atoms for different methods.

Index	True 1	True 2	True 3	Ghost 1	Ghost 2	Ghost 3
Real atoms	[3, 0.23]	[4, −0.08]	[9, −0.22]	[6, 0.46]	[7, 0.15]	[8, −0.16]
LSA	[3, 0.234]	[4, −0.0795]	[9, −0.2164]	[6, 0.4738]	[7, 0.1773]	[1, 0.05]
Proposed method	[3, 0.2328]	[4, −0.0805]	[9, −0.218]	[6, 0.4727]	[7, 0.1758]	[8, −0.1797]

Figure 5 presents the SINR loss performances of the proposed algorithm and three existing methods along the main beam direction. The normalized Doppler frequencies span from −0.5 to 0.5. From the simulation results, we find that STAP has nulls both in the DP clutter area (normalized Doppler frequencies of −0.5 and 0.5) and the MP clutter area (normalized Doppler frequencies of −0.23, 0.08, 0.22, −0.46, −0.15 and 0.16), while the other methods exhibit nulls only in the DP clutter area. This is because SRA, LSA, and the proposed approach effectively cancel the MP clutter before DP clutter suppression. As a consequence, the SINR loss performance in the non-DP clutter region reflects the MP clutter suppression capability. Furthermore, it is also shown from Figure 5 that the proposed algorithm provides a better SINR loss performance than LSA and SRA. This is because the proposed algorithm adds the ICM-MP error calibration step to mitigate its effect on MP profile estimation compared with LSA and addresses the off-grid and ICM problems compared with SRA.

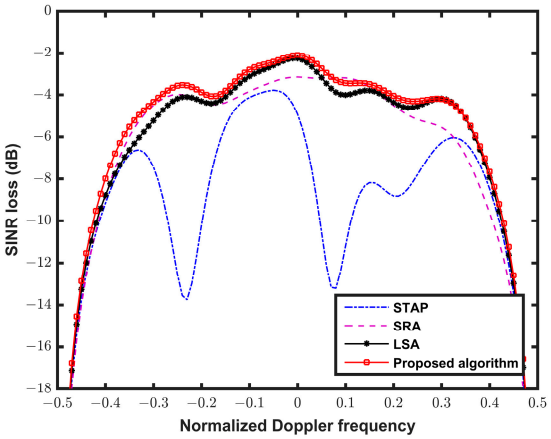


Figure 5. SINR loss performances of different methods.

Figure 6 presents the target detection results for different methods. Snapshots from the 992th to 1008th range cells are filtered in each method. It is found that STAP yields the worst target detection performance because the target located in the MP clutter region is also canceled. Moreover, SRA and LSA suffer from some performance loss in the presence of ICM-MP fluctuation when compared with the proposed algorithm. Therefore, it is concluded from the third experiment that the proposed joint optimization approach can provide satisfactory cancellation capability and detection performance in the presence of ICM-MP fluctuation and off-grid issues.

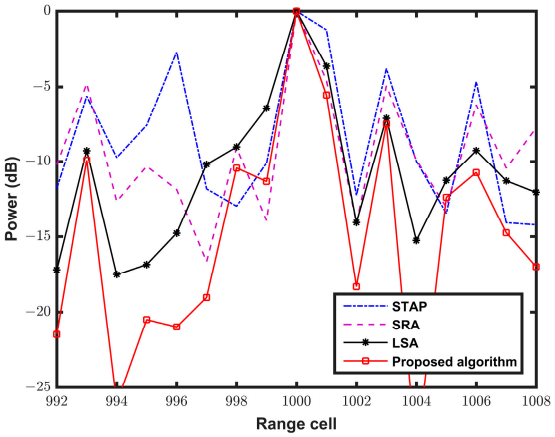


Figure 6. Target detection performance versus range cell for different methods.

In the fourth experiment, we compare the performance of the proposed joint optimization algorithm with other existing methods in different ICM-MP scenarios. First, we consider three ICM-MP scenarios, namely no ICM-MP fluctuation, that is, $\sigma_{2,v} = 0$, $\sigma_{2,v} = 0.8$, and $\sigma_{2,v} = 1.6$. In the simulation, the MDR of three MP signals is -20 dB, and the remaining simulation parameters are the same as in the third experiment.

Figure 7 presents the SINR loss performance against the normalized Doppler frequency in different ICM-MP scenarios. From the simulation results, it is found that SRA, LSA, and the proposed algorithm outperform STAP regardless of the presence or absence of the ICM-MP fluctuation. Moreover, the SINR loss performance of SRA suffers a lot in these three cases. The reason is that the presence of ICM-MP fluctuations and off-grid problems disturbs the MP clutter estimation in SRA, leading to a severe SINR performance loss. Moreover, the SINR loss performance of LSA changes obviously with respect to ICM-MP fluctuations. Especially as the velocity standard deviation $\sigma_{2,v}$ increases, the performance of LSA becomes worse. This is because the accuracy of the selected atoms and estimated profile in LSA is sensitive to the ICM-MP fluctuation. Conversely, the proposed joint optimization algorithm always features acceptable SINR loss performance, whether the ICM-MP fluctuation is present or not.

In Figure 8, we present the corresponding detection results of the proposed joint optimization approach and the other three methods. The results illustrate that STAP yields substandard detection performance, and SRA no longer performs properly even in the absence of CIM-MP fluctuation. Additionally, as $\sigma_{2,v}$ increases, the detection performance of LSA improves. However, the proposed algorithm still provides satisfactory detection performance.

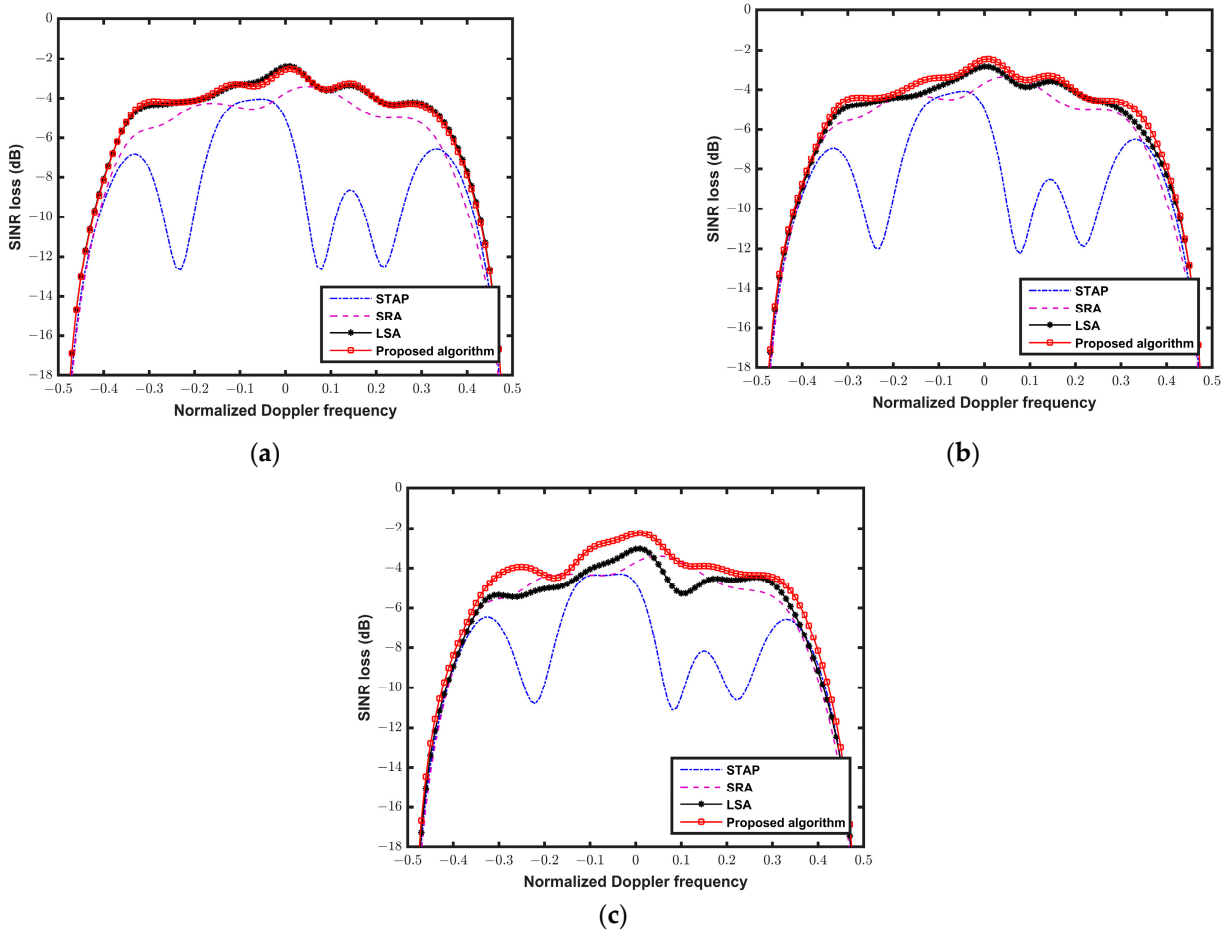


Figure 7. Impacts of ICM-MP fluctuation on SINR loss performance of the proposed algorithm and the existing methods. (**a**) $\sigma_{2,v} = 0$; (**b**) $\sigma_{2,v} = 0.8$; (**c**) $\sigma_{2,v} = 1.6$.

Then, we make a quantitative comparison between the proposed algorithm, SRA, and LSA with different ICM-MP fluctuations, i.e., $\sigma_{2,v} = 0.2$, 0.6, 1.0, 1.4, and 1.8. The SINR loss value at the target Doppler frequency considering different $\sigma_{2,v}$ is listed in Table 3. It is clear that the proposed joint optimization method can cope with the off-grid issues and is robust to the ICM-MP fluctuation.

Table 3. The SINR loss value at the target Doppler frequency with different $\sigma_{2,v}$.

$\sigma_{2,v}$	**0.2**	**0.6**	**1.0**	**1.4**	**1.8**
SRA (dB)	−5.046	−5.032	−5.097	−5.104	−5.096
LSA (dB)	−4.451	−4.827	−5.115	−5.481	−5.668
Proposed algorithm (dB)	−4.278	−4.321	−4.318	−4.432	−4.417

In the fifth experiment, the SINR loss performances of different approaches with different MDR values are discussed. Figure 9 presents the SINR loss performances of different algorithms. In the simulation, we consider three MP signals having the same MDR values and set the MDR values as −22 dB and −17 dB, respectively. Other simulation parameters are the same as the third experiment.

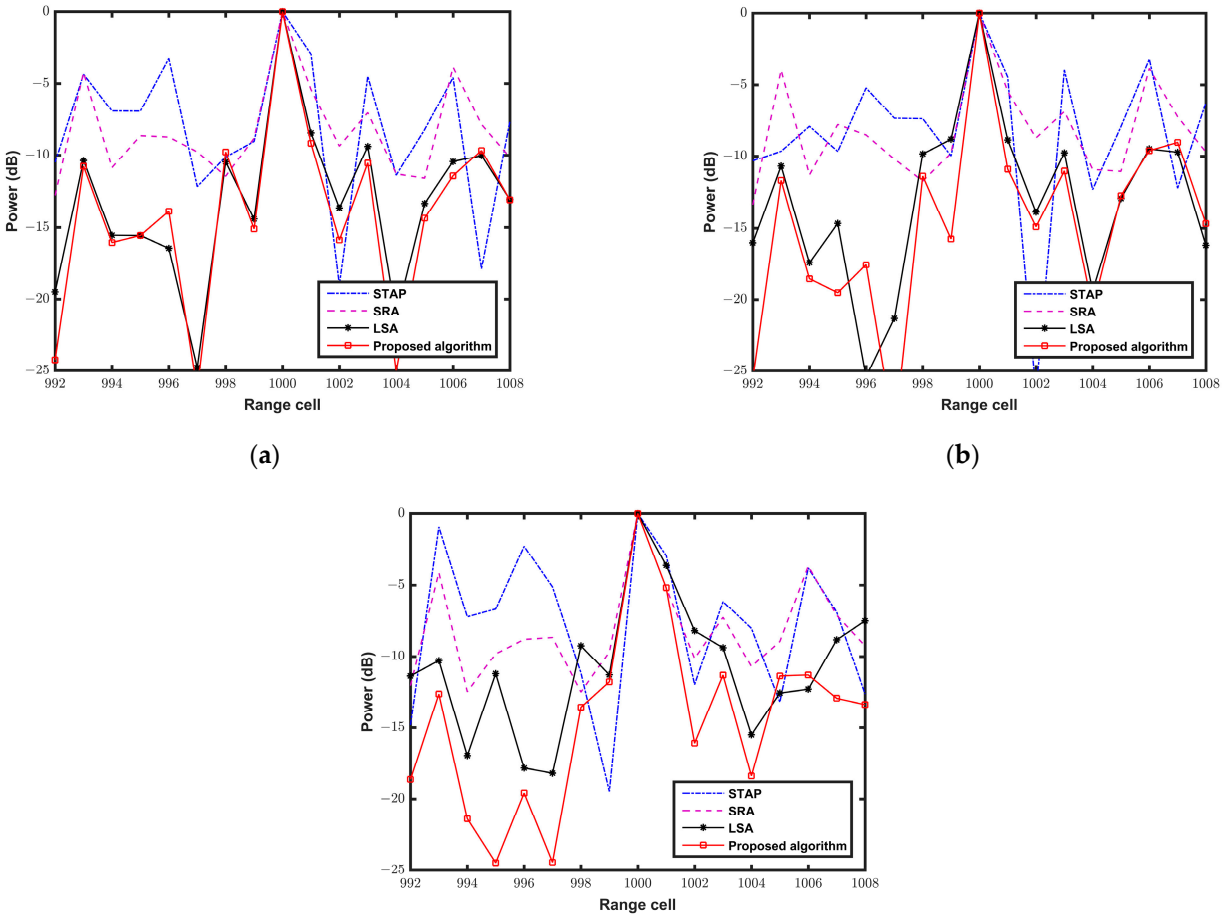


Figure 8. Impacts of ICM-MP fluctuation on target detection performance of the proposed algorithm and the existing methods. (**a**) $\sigma_{2,v} = 0$; (**b**) $\sigma_{2,v} = 0.8$; (**c**) $\sigma_{2,v} = 1.6$.

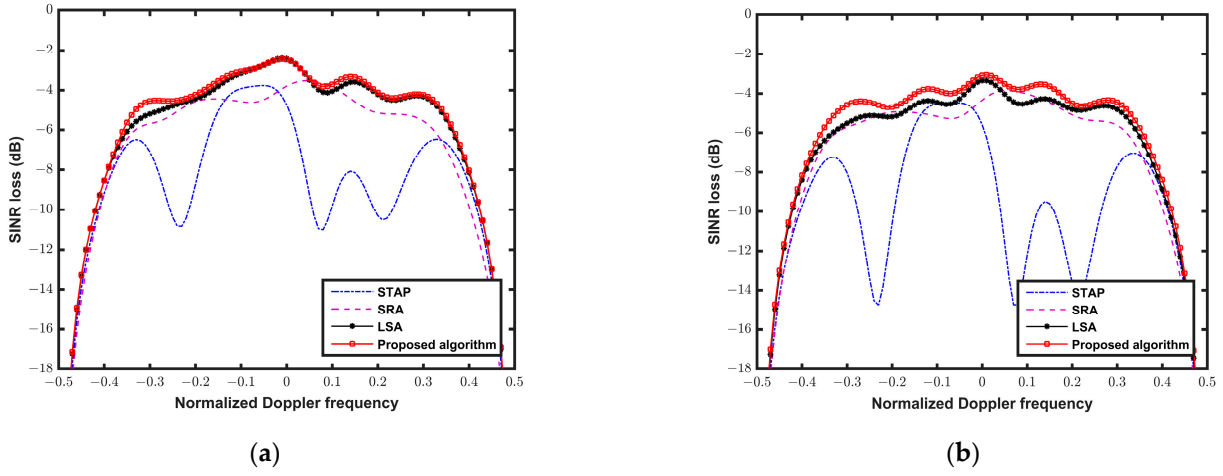


Figure 9. Impacts of MDR on SINR loss performance of the proposed algorithm and the existing methods. (**a**) MDR = −22 dB; (**b**) MDR = −17 dB.

It is seen from Figure 9 that the SINR loss performances of STAP and LSA vary obviously with MDR, and the SINR loss performance deteriorates with an increasing MDR value. The reason is that the high MDR causes deep nulls in the MP clutter area for STAP and residual MP clutter in profile estimation for LSA. Additionally, SRA provides

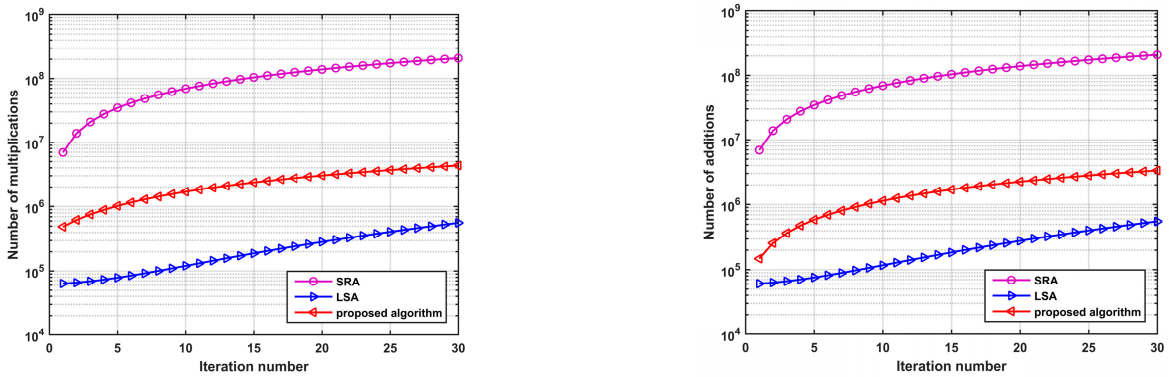
substandard performance, and the performance degradation is due to the off-grid issue and the ICM problem. Conversely, the proposed joint optimization approach provides superior SINR loss performance in these two MDR scenarios.

Then, the proposed algorithms, SRA and LSA, are compared quantitatively. Table 4 represents the SINR loss values at the target Doppler frequency considering different MDR values, i.e., MDR = −15 dB, −19 dB, −23 dB, −27 dB, and −31 dB, respectively. It is found from Table 4 that the proposed approach provides enhanced SINR loss performance compared to SRA and LSA when the MDR value changes. Therefore, it is concluded that regardless of the MDR values, the proposed algorithm can resolve the off-grid issue and is robust to the ICM-MP fluctuation.

Table 4. The SINR loss value at the target Doppler frequency with different MDR values.

MDR Value (dB)	−15	−19	−23	−27	−31
SRA (dB)	−5.321	−5.032	−4.957	−4.915	−4.876
LSA (dB)	−5.228	−4.867	−4.565	−4.348	−4.084
Proposed algorithm (dB)	−4.656	−4.444	−4.268	−4.032	−4.081

Finally, we evaluate the computational complexities of different algorithms. The computational complexity of the proposed algorithm is discussed in Section 4.4, and the computational complexity of SRA and LSA has been analyzed in references [10,11]. The simulation results are presented in Figure 10. The curves indicate that the proposed algorithm has lower computational complexity than SRA. This is because the inverse operation of the high-dimensional matrix is computationally intensive for SRA. In addition, the proposed algorithm has mildly higher complexities than LSA due to the dictionary updating and the added calibration step. However, the proposed algorithm outperforms LSA in MP clutter suppression, which was presented in the previous experiments. Therefore, it is concluded that the proposed algorithm has satisfactory suppression performance and moderate complexity in the presence of ICM-MP errors.



(**a**) (**b**)

Figure 10. Computational complexities of different algorithms. (**a**) number of multiplications; (**b**) number of additions.

6. Conclusions

In the presence of ICM-MP fluctuations, the existing sparse model of MP clutter is disturbed, and the performance of the existing MP clutter suppression methods drops. In this paper, a MP clutter cancellation approach is presented to eliminate the influence of ICM-MP fluctuation. The proposed algorithm modifies the sparse model of MP clutter, derives a joint optimization problem, and alternately estimates the ICM-MP fluctuations and MP clutter profile with off-grid effects mitigation. The experimental results indicate the proposed joint optimization algorithm outperforms the existing STAP, LSA, and RSA in

MP clutter cancellation when ICM-MP fluctuation exists. Moreover, the proposed approach can deal with the off-grid issue and is robust to the ICM-MP fluctuation, regardless of the MDR values.

By ignoring the influence of range ambiguities, the proposed algorithm can suppress MP clutter with ICM-MP calibration. However, the assumption may be violated in practice, and the performance of the proposed algorithm may degrade. Consequently, extending our model by considering range ambiguities is the research direction of our future work. In addition, possible future studies include robust MP clutter suppression in nonhomogeneous and nonstationary clutter environments for airborne passive radar.

Author Contributions: Formal analysis, Y.D. and Z.P.; methodology, Y.D. and Z.P.; validation, Y.D. and W.L.; writing—original draft, Y.D.; writing—review and editing, W.L. and D.J. All authors have read and agreed to the published version of the manuscript.

Funding: This research was funded by the Hunan Provincial Natural Science Foundation of China, grant No. 2021JJ40029; Scientific Research Fund of the Hunan Provincial Education Department, grant No. 21B0710; and the 2021 Undergraduate Innovation and Entrepreneurship Training Program of Hunan Province, grant No. 3333.

Institutional Review Board Statement: Not applicable.

Informed Consent Statement: Not applicable.

Data Availability Statement: Data sharing is not applicable to this article.

Conflicts of Interest: The authors declare no conflict of interest.

References

1. Malanowski, M.; Rytel-Andrianik, R.; Kulpa, K.; Stasiak, K.; Ciesielski, M.; Kulpa, J. Geometric clutter analysis for airborne passive coherent location radar. *IEEE Trans. Geosci. Remote Sens.* **2022**, *60*, 5116314. [CrossRef]
2. Tan, D.K.P.; Lesturgie, M.; Sun, H.; Lu, Y. Space–time interference analysis and suppression for airborne passive radar using transmissions of opportunity. *IET Radar Sonar Navig.* **2014**, *8*, 142–152. [CrossRef]
3. Wojaczek, P.; Colone, F.; Cristallini, D.; Lombardo, P. Reciprocal-Filter-Based STAP for Passive Radar on Moving Platforms. *IEEE Trans. Aerosp. Electron. Syst.* **2019**, *55*, 967–988. [CrossRef]
4. Rosenberg, L.; Duk, V. Land clutter statistics from an airborne passive bistatic radar. *IEEE Trans. Geosci. Remote Sens.* **2022**, *60*, 5104009. [CrossRef]
5. Sui, J.; Wang, J.; Zuo, L.; Gao, J. Cascaded least square algorithm for strong clutter removal in airborne passive radar. *IEEE Trans. Aerosp. Electron. Syst.* **2022**, *58*, 679–696. [CrossRef]
6. Brown, J.; Woodbridge, K.; Griffiths, H.; Stove, A.; Watts, S. Passive bistatic radar experiments from an airborne platform. *IEEE Aerosp. Electron. Syst. Mag.* **2012**, *27*, 50–55. [CrossRef]
7. Sui, J.; Wang, J.; Zuo, L.; Gao, J. Multistage least squares algorithms for clutter suppression in airborne passive radar based on subband operation. *IEEE Trans. Aerosp. Electron. Syst.* **2023**, *59*, 1893–1909. [CrossRef]
8. Deng, Y.; Wang, J.; Luo, Z.; Guo, S. Cascaded suppression method for airborne passive radar with contaminated reference signal. *IEEE Access* **2019**, *7*, 50317–50329. [CrossRef]
9. Guo, S.; Wang, J.; Ma, H.; Wang, J. Modified blind equalization algorithm based on cyclostationarity for contaminated referent signal in airborne PBR. *Sensors* **2020**, *20*, 788. [CrossRef]
10. Deng, Y.; Zhang, S.; Zhu, Q.; Zhang, L.; Li, W. Clutter suppression methods based on reduced-dimension transformation for airborne passive radar with impure reference signals. *J. Appl. Remote Sens.* **2021**, *15*, 016514. [CrossRef]
11. Deng, Y.; Li, W.; Zhang, S.; Wang, F.; Xiao, W.; Cui, Z. Clutter suppression method for off-grid effects mitigation in airborne passive radars with contaminated reference signals. *Sensors* **2021**, *21*, 6339. [CrossRef]
12. Ward, J. Space-Time Adaptive Processing for Airborne Radar. In Proceedings of the IEE Colloquium on Space-Time Adaptive Processing, London, UK, 6 April 1998.
13. Klemm, R. *Principles of Space-Time Adaptive Processing*, 3rd ed.; Institute of Electical Engineering: London, UK, 2006.
14. Mevin, W.L.; Showman, G.A. An approach to knowledge-aided covariance estimation. *IEEE Trans. Aerosp. Electron. Syst.* **2006**, *42*, 1021–1042. [CrossRef]
15. Liu, M.; Zou, L.; Yu, X.; Zhou, Y.; Wang, X.; Tang, B. Knowledge aided covariance matrix estimation via gaussian Kernel function for airborne SR-STAP. *IEEE Access* **2020**, *8*, 5970–5978. [CrossRef]
16. Riedl, M.; Potter, L.C. Multimodel shrinkage for knowledge-aided space-time adaptive processing. *IEEE Trans. Aerosp. Electron. Syst.* **2018**, *54*, 2601–2610. [CrossRef]

17. Hu, J.; Li, J.; Li, H.; Li, K.; Liang, J. A novel covariance matrix estimation via cyclic characteristic for STAP. *IEEE Geosci. Remote Sens. Lett.* **2020**, *17*, 1871–1875. [CrossRef]
18. Liu, C.; Wang, T.; Zhang, S.; Ren, B. A clutter suppression algorithm via weighted l_2-norm penalty for airborne radar. *IEEE Signal Process. Lett.* **2022**, *29*, 1522–1525. [CrossRef]
19. Zhou, Y.; Wang, L.; Chen, X.; Wen, C.; Jiang, B.; Fang, D. An improving EFA for clutter suppression by using the persymmetric covariance matrix estimation. *Circuits Syst. Signal Process.* **2018**, *37*, 4136–4149. [CrossRef]
20. Cui, N.; Duan, K.; Xing, K.; Yu, Z. Beam-space reduced-dimension 3D-STAP for nonside-looking airborne radar. *IEEE Geosci. Remote Sens. Lett.* **2022**, *19*, 3506505. [CrossRef]
21. Shen, S.; Tang, L.; Nie, X.; Bai, Y.; Zhang, X.; Li, P. Robust space time adaptive processing methods for synthetic aperture radar. *Appl. Sci.* **2020**, *10*, 3609. [CrossRef]
22. Shen, M.; Zhu, D.; Zhu, Z. Reduced-rank space-time adaptive processing using a modified projection approximation subspace tracking deflation approach. *IET Radar Sonar Navig.* **2009**, *3*, 93–100. [CrossRef]
23. Huang, P.; Zou, Z.; Xia, X.; Liu, X.; Liao, G. A novel dimension-reduced space–time adaptive processing algorithm for spaceborne multichannel surveillance radar systems based on spatial–temporal 2-D sliding window. *IEEE Trans. Geosci. Remote Sens.* **2022**, *60*, 5109721. [CrossRef]
24. Shi, J.; Xie, L.; Cheng, Z.; He, Z.; Zhang, W. Angle-Doppler channel selection method for reduced-dimension STAP based on sequential convex programming. *IEEE Comm. Lett.* **2021**, *25*, 3080–3084. [CrossRef]
25. Chen, W.; Xie, W.; Wang, Y. Short-range clutter suppression for airborne radar using sparse recovery and orthogonal projection. *IEEE Geosci. Remote Sens. Lett.* **2022**, *19*, 3500605. [CrossRef]
26. Xie, L.; He, Z.; Tong, J.; Zhang, W. A recursive angle-Doppler channel selection method for reduced-dimension space-time adaptive processing. *IEEE Trans. Aerosp. Electron. Syst.* **2020**, *56*, 3985–4000. [CrossRef]
27. Yang, Z.; de Lamare, R.C.; Li, X. L1-regularized STAP algorithms with a generalized sidelobe canceler architecture for airborne radar. *IEEE Trans. Signal Process.* **2012**, *60*, 674–686. [CrossRef]
28. Wang, X.; Yang, Z.; Huang, J.; de Lamare, R.C. Robust two-stage reduced-dimension sparsity-aware STAP for airborne radar with coprime arrays. *IEEE Trans. Signal Process.* **2020**, *68*, 81–96. [CrossRef]
29. Li, X.; Yang, X.; Wang, Y.; Duan, K. Gridless sparse clutter nulling STAP based on particle swarm optimization. *IEEE Geosci. Remote Sens. Lett.* **2022**, *19*, 4023205. [CrossRef]
30. Zhang, W.; An, R.; He, N.; He, Z.; Li, H. Reduced dimension STAP based on sparse recovery in heterogeneous clutter environments. *IEEE Trans. Aerosp. Electron. Syst.* **2020**, *56*, 785–795. [CrossRef]
31. Hu, Z.; Wang, W.; Dong, F. A low-complexity MIMO radar STAP strategy for efficient sea clutter suppression. *IEEE Geosci. Remote Sens. Lett.* **2022**, *19*, 4024105. [CrossRef]
32. Cui, N.; Xing, K.; Yu, Z.; Duan, K. Tensor-based sparse recovery space-time adaptive processing for large size data clutter suppression in airborne radar. *IEEE Trans. Aerosp. Electron. Syst.* **2023**, *59*, 907–922. [CrossRef]
33. Duan, K.; Chen, H.; Xie, W.; Wang, Y. Deep learning for high-resolution estimation of clutter angle-Doppler spectrum in STAP. *IET Radar Sonar Navig.* **2022**, *16*, 193–207. [CrossRef]
34. Zou, B.; Wang, X.; Feng, W.; Zhu, H.; Lu, F. DU-CG-STAP method based on sparse recovery and unsupervised learning for airborne radar clutter suppression. *Remote Sens.* **2022**, *14*, 3472. [CrossRef]
35. Yang, Z.; Qin, Y.; de Lamare, R.C.; Wang, H.; Li, X. Sparsity-based direct data domain space-time adaptive processing with intrinsic clutter motion. *Circuits Syst. Signal Process.* **2017**, *36*, 219–246. [CrossRef]
36. Yang, Z.; Li, X.; Wang, H.; Fa, R. Knowledge-aided STAP with sparse-recovery by exploiting spatio-temporal sparsity. *IET Signal Process.* **2016**, *10*, 150–161. [CrossRef]
37. Gu, Y.; Wu, J.; Fang, Y.; Zhang, L.; Zhang, Q. End-to-end moving target indication for airborne radar using deep learning. *Remote Sens.* **2022**, *14*, 5354. [CrossRef]
38. Duan, K.; Liu, W.; Duan, G.; Wang, Y. Off-grid effects mitigation exploiting knowledge of the clutter ridge for sparse recovery STAP. *IET Radar Sonar Navig.* **2018**, *12*, 557–564. [CrossRef]
39. Ma, Z.; Liu, Y.; Meng, H.; Wang, X. Sparse recovery-based space-time adaptive processing with array error self-calibration. *Electron. Lett.* **2014**, *50*, 952–954. [CrossRef]
40. Yang, Z.; de Lamare, R.C.; Liu, W. Sparsity-based STAP using alternating direction method with gain/phase errors. *IEEE Trans. Aerosp. Electron. Syst.* **2017**, *53*, 2756–2768.

Disclaimer/Publisher's Note: The statements, opinions and data contained in all publications are solely those of the individual author(s) and contributor(s) and not of MDPI and/or the editor(s). MDPI and/or the editor(s) disclaim responsibility for any injury to people or property resulting from any ideas, methods, instructions or products referred to in the content.